THE JOURNAL OF PHYSICAL CHEMISTRY Letters

pubs.acs.org/JPCL Letter

Electronic Structures and Surface Reconstructions in Magnetic Superconductor $RbEuFe_4As_4$

Vasily S. Stolyarov,* Kirill S. Pervakov, Anna S. Astrakhantseva, Igor A. Golovchanskiy, Denis V. Vyalikh, Timur K. Kim, Sergey V. Eremeev, Vladimir A. Vlasenko, Vladimir M. Pudalov, Alexander A. Golubov, Eugene V. Chulkov, and Dimitri Roditchev

Cite This: J. Phys. Chem. Lett. 2020, 11, 9393−9399 Read Online

ACCESS | Metrics & More | Article Recommendations | Supporting Information

ABSTRACT: In pnictide $RbEuFe_4As_4$, superconductivity sets in at 36 K and coexists, below 15−19 K, with the long-range magnetic ordering of Eu 4f spins. Here we report scanning tunneling experiments performed on cold-cleaved single crystals of the compound. The data revealed the coexistence of large Rb-terminated and small Eu-terminated terraces, both manifesting 1×2 and $\sqrt{2} \times \sqrt{2}$ reconstructions. On $\sqrt{2} \times \sqrt{2}$ surfaces, a hidden electronic order with a period ∼5 nm was discovered. A superconducting gap of ∼7 meV was seen to be strongly filled with quasiparticle states. The tunneling spectra compared with density functional theory calculations confirmed that flat electronic bands due to Eu 4f orbitals are situated ∼1.8 eV below the Fermi level and thus do not contribute directly to Cooper pair formation.

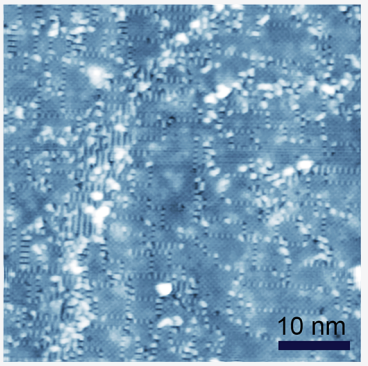

Until recently, the interplay between magnetism and superconductivity[1−5] was experimentally studied mainly in a few exotic materials such as UGe_2, URhGe, and UCoGe,[6,7] in which a triplet superconductivity is probably in play. In the so-called 122 iron-based materials AFe_2As_2, where A = Ba, Sr, Ca, etc.,[8,9] the use of the rare-earth element Eu leads to magnetism,[10] while preserving singlet superconductivity.[11,12] For example, in $EuFe_2(As_{1-x}P_x)_2$, the substitutional doping by phosphorus results, at $x \sim 0.2$, in superconductivity at a rather high critical temperature (T_c) of 25−28 K; below a T_{Curie} of 15−20 K, it coexists with the ferromagnetic order of Eu subsystems.[11−20] This unique coexistence rapidly became the subject of intensive studies. Novel ferromagnetic superconducting phases, such as the domain Meissner state and domain vortex state, were discovered;[16,18] a peculiar interplay was observed in the microwave response,[19] and a crossover from a dominating superconducting to a dominating ferromagnetic order was reported.[20]

The magnetic superconductor $RbEuFe_4As_4$ has a more complex structure, alternating Eu-122 and Rb-122 blocks.[21−27] This stoichiometric compound is characterized by a higher T_c of ≈36 K and a slightly lower T_{Curie} of ≈15−19 K, compared to those of $EuFe_2(As_{1-x}P_x)_2$. The magnetic order of $RbEuFe_4As_4$ is also different. Below the Curie temperature, it is expected to be a helical antiferromagnet rather than a ferromagnet[28] and even can have topological magnetic order.[29] The interplay between the two orders in $RbEuFe_4As_4$ is currently being hotly debated; several experimental[30−34] and theoretical[35,36] studies have recently reported been and suggested a singlet superconductivity.[35,37,38]

In the past, 122 materials were extensively studied by different experimental means, including scanning tunneling microscopy and spectroscopy (STM/STS).[39−41] Ba-122 doped with Co, Ni, or Cr[40−49] or Sr-122 and Ca-122[39,40,50,51] all demonstrated 1×2 and $\sqrt{2} \times \sqrt{2}$[42−44,46,50,51] surface reconstructions, both corresponding to the half-coverage of the topmost layer by Ba, Sr, or Ca.[40] The superconducting gaps in the tunneling spectra were observed to be strongly filled with quasiparticle states. An intriguing nematic order was revealed.[39] However, tunneling studies of magnetic superconducting pnictides and, specifically, of $RbEuFe_4As_4$ are missing, mainly due a low crystal quality and a poor morphology of cleaved surfaces, making STM/STS experiments challenging.

In this paper, we present low-temperature (1.5−35 K) STM/STS measurements of high-quality single crystals of $RbEuFe_4As_4$.[53] The experimental difficulties mentioned above were resolved by cooling the samples to 4.2 K and in situ cleaving them (to limit atom diffusion and avoid a strong

Received: September 6, 2020
Accepted: October 12, 2020
Published: October 23, 2020

surface modification), thus achieving large atomically smooth terraces (see Sample preparation and STM study in the Supporting Information). All terraces demonstrate 1 × 2 and $\sqrt{2} \times \sqrt{2}$ surface reconstructions that coexist at the nanoscale. Despite identical reconstructions, the terraces have different atomic compositions. They are either Rb- or Eu-terminated. By comparing STM results with STS data and density functional theory (DFT) calculation, we found that most of the exposed surface is Rb-terminated while only a few terraces are Eu-terminated. In the regions with $\sqrt{2} \times \sqrt{2}$ reconstruction, STS revealed a spatial ordering of occupied electronic states with a surprisingly large period of ∼5 nm. At the Fermi level, a signature of a superconducting gap of ∼7 meV was observed in the tunneling conductance spectra. The gap appears to be strongly filled with quasiparticle excitations and characterized by smeared coherence peaks.

Constant current STM images revealed atomically flat terraces separated by sharp steps (Figure 1a). The height of the steps among terraces A, B, and D is ≃1.3 nm (see the inset of Figure 1a), matching the unit cell height of $RbEuFe_4As_4$[23−27] (Figure 1b). Terrace C is situated 0.66 nm above terrace B. This corresponds to the half-unit cell of the material. This points toward the coexistence of Rb- and Eu-terminated surfaces (A, B, and D, Rb-terminated; C, Eu-terminated), as we discuss below. Statistically, single-unit cell steps are dominant.

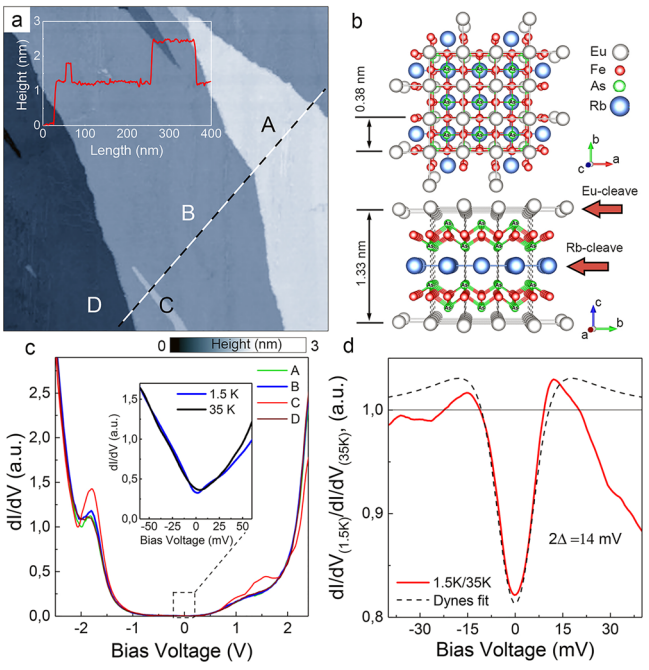

Figure 1. Scanning tunneling microscopy and spectroscopy of $RbEuFe_4As_4$. (a) A 400 nm × 400 nm STM image (bias voltage V_T = −1.5 V, and tunnel current I_T = −90 pA) of the cold-cleaved sample. Atomically flat terraces A, B, and D are separated by ≃1.3 nm high steps; the height of terrace C with respect to terrace B is ≃0.66 nm. The inset shows a plot of a STM scan profile along the white dashed line. (b) Crystal structure of $RbEuFe_4As_4$. Red arrows show expected cleavage planes. (c) Terrace-averaged tunneling conductance curves acquired in regions A (green), B (blue), C (red), and D (brown line). The inset shows the tunneling DOS measured at 35 K (black line) and 1.5 K (blue line). (d) The red solid line shows the normalized tunneling conductance $dI/V(V)_{T=1.5K}/dI/V(V)_{T=35K}$ near zero bias, and the black dashed line the best fit by the Dynes formula.[52] The fit parameters are as follows: Δ_{fit} = 6.8 mV, and Γ_{fit} = 9.5 mV (see the text).

Typical tunneling conductance spectra $dI(V)/dV$ acquired on terraces A−D are presented in Figure 1c. Being similar, they are all characterized by a rather low spectral density around the Fermi level, by a sharp peak at $V_T \simeq -1.8$ V, two bumps at 1.0 and 1.5 V, and by a rapid spectral rise at higher biases. The peaks have a stronger amplitude in the spectra acquired on terrace C (red curve). The inset of Figure 1c focuses on a narrower spectral window around the Fermi level. A robust feature here is a pronounced asymmetric V-like spectral shape (the presented blue spectrum was acquired on terrace B, but other terraces present similar spectra). The V shape is preserved at high temperatures (black line) and, as we will see below, reflects a complex multiband electronic structure of the material.[28,32]

Another robust feature is the evolution of the temperature of the tunneling conductance spectra near zero bias, visible in inset of Figure 1c. As the temperature is decreased, the spectral weight at zero bias decreases and bumps appear at approximately ±15 mV. Because of a strongly energy-dependent normal-state electronic density of states in $RbEuFe_4As_4$ (unlike in simple metals), the redistribution of electronic states around the Fermi level is better revealed in the normalized tunneling conductance spectra $dI/V(V)_{T=1.5K}/dI/V(V)_{T=35K}$, presented in Figure 1d. When the STS spectra are acquired in different locations, the dip at zero bias followed by peaks at both polarities is ubiquitous, while the overall spectral background is subject to variations (we discuss this point below). The spectral features in Figure 1d are characteristic of a superconducting gap with a width Δ of ≃7 ± 2 meV. Though the shape of the gap is unconventional, the peaks are large and strongly smeared, and the gap is not complete. Even at 1.5 K, only ∼15% of the total electronic states at the Fermi level are gapped.

By now, we focus on the atomic order observed on terraces. Similar to 122 pnictides, $RbEuFe_4As_4$ is a strongly anisotropic lamellar material (Figure 1b). In the $a-b$ plane, it has an orthorhombic, almost square 0.39 nm wide unit cell (the differences between directions a and b are tiny: a_0 = 0.39382 nm, and b_0 = 0.38975 nm[27]). In direction c, alternating Rb and Eu atomic layers are sandwiched by As−Fe_2−As blocks. Rb and Eu layers are weak links of the structure; during sample cleavage, the structure breaks following these layers, thus presenting c-oriented surfaces. The observed predominance of single-unit cell high steps over half-unit cell ones in Figure 1a points toward the difference in the binding energy between Rb and Eu layers. Our estimations (see DFT calculations in the Supporting Information) show that Rb−As and Eu−As binding energies are indeed different (0.27 and 0.47 eV, respectively). During sample cleavage, one expects the weakest bonds to break. We thus may suppose that the majority of the cleaved surface is Rb-terminated and conclude that terraces A, B, and D are Rb-terminated and terrace C is Eu-terminated.

A detailed STM study of the terrace's structures revealed the coexistence of two different surface reconstructions. The first one is a striped reconstruction (Figure 2a,b); it is largely dominant on all studied terraces. The analysis of this structure (Figure 2c), enables identifying it as a 1 × 2 reconstruction,[40] which was already observed in several 122 pnictides.[42,44,50] The chains follow direction a or b; the boundaries between perpendicularly oriented domains are easily detected in STM images (Figure 2a). The second reconstruction is identified as

https://dx.doi.org/10.1021/acs.jpclett.0c02711
J. Phys. Chem. Lett. 2020, 11, 9393−9399

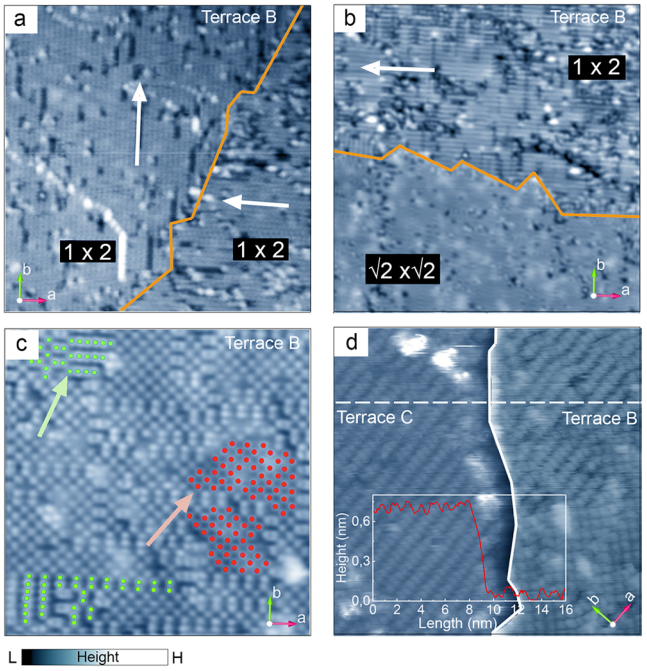

Figure 2. Surface reconstruction. (a) A 46 nm × 46 nm STM image (bias $V_T = -200$ mV, and tunnel current $I_T = -100$ pA). Atomically flat terraces are 1 × 2 reconstructed; 1 × 2 chains are aligned in the *a* or *b* direction and form domains. (b) A 50 nm × 50 nm STM image ($V_T = -200$ mV, and $I_T = -400$ pA). A majority of 1 × 2 chain domains coexist with minority domains of the 1 × 2 reconstruction. White arrows show the orientation of reconstruction domains $\sqrt{2} \times \sqrt{2}$, and the solid orange line corresponds to the domain boundaries. (c) A 20 nm × 20 nm STM image ($V_T = 20$ mV, and $I_T = 1.9$ nA) demonstrates the coexistence of both reconstructions on a atomic scale. Green and orange circles are guides for the eye. Selected stacking faults of 1 × 2 and $\sqrt{2} \times \sqrt{2}$ reconstructions are denoted by arrows. (d) A 16 nm × 16 nm STM image in the vicinity of the half-unit cell step (solid white line) between regions C (left) and B (right). An offset was applied to the image in region B to make atomic orders visible on both sides. The inset shows a STM scan profile over the C/B step.

a 45° rotated $\sqrt{2} \times \sqrt{2}$ square one[40] (Figure 2c). Typical defects such as voids and stacking faults (pointed by arrows) are observed in both reconstructions. Amazingly, the stacking faults of the $\sqrt{2} \times \sqrt{2}$ structure form clusters of the 1 × 2 reconstruction and verse versa. The defect density is high; by approaching the STM tip or changing the bias, they can be easily moved and rearranged. This is clearly seen by comparing the STM image in Figure 2b with the image of the same region acquired during the STS experiment (Figure 4a). In these images, both reconstructions are present: the upper part of the image is 1 × 2-covered, while the lower part is $\sqrt{2} \times \sqrt{2}$ reconstructed. Both reconstructions correspond to the same 1/2 atomic layer density (see also Supplementary Figure 1).

The reconstructions observed on terraces B and C are quite similar, as the STM image presented in Figure 2d demonstrates. It focuses on the step region between the two terraces. In the left part of the image, terrace C presents the 1 × 2 reconstruction; in the right part of the same image, terrace B presents both 1 × 2 (top part) and $\sqrt{2} \times \sqrt{2}$ (bottom part) reconstructions. Thus, 1 × 2 and $\sqrt{2} \times \sqrt{2}$ reconstructions are less sensitive to the nature of the topmost atoms than to the underlying As−Fe_2−As template.

It is tempting to relate the observed spectral features (Figure 1c) to the electronic structure of the material. In Figure 3, we

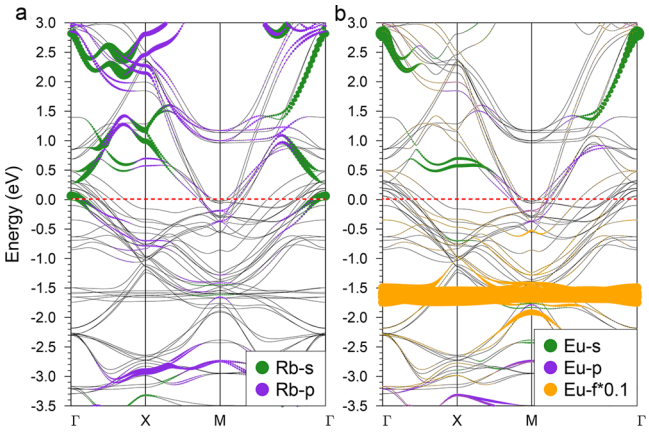

Figure 3. Calculated electronic structure of $RbEuFe_4As_4$. The size of the colored circles in the panels represents the relative weight of specific (a) Rb and (b) Eu orbitals. In panel b, the relative weight of the Eu 4f orbitals is artificially reduced by a factor of 10 with respect to other orbitals, for the sake of clarity. The red dashed line corresponds to the Fermi energy.

present the electronic bands of bulk $RbEuFe_4As_4$ calculated within the DFT+U framework (see DFT calculations in the Supporting Information). There, different colors represent the weights of different Rb and Eu atomic orbitals in the band structure (the weights of Fe and As orbitals are available in Supplementary Figure 2). An expected feature is a bunch of hole-like bands situated around the M-point of the Brillouin zone that overlaps in energy with several holelike bands centered at the Γ-point. The dispersion slope $|\partial E/\partial k|$ is rather high for both sets of bands, resulting in a low density of states. At higher (positive and negative) energies, several flatter bands add their spectral weight to the total DOS. This is consistent with the observed overall V-shaped spectral background (Figure 1c). A very interesting result of the DFT calculations is a flat band around −1.7 eV, mainly due to Eu 4f orbitals (colored yellow in Figure 3, right panel). Such a band could be responsible for the spectral peak observed at $V_T \simeq -1.8$ V. Moreover, as part of this hypothesis, a higher peak amplitude observed on terrace C could be associated with Eu termination at the surface, in agreement with our expectations. The fact that most of the spectral density coming from magnetic Eu is situated deep below the Fermi level is an important indication that Eu does not contribute directly to Cooper pair formation in $RbEuFe_4As_4$.

The identification of humps at V_T values of ≃1.0 and ≃1.5 V is more complicated. Some flat bands indeed exist at these energies (at 0.6 eV around the X-point, at 0.9 eV around the Γ-point, and at 1.3 eV around the M-point), but DFT predicts most of states to come from Fe (see Supplementary Figure 2), which is in the same configuration for both considered surface terminations. Moreover, the contributions from Rb and Eu orbitals are predicted to be similar. The reasons why these peaks are better revealed on terrace C might be related to surface states that could be different in the case of Rb- and Eu-terminated surfaces or yet to slightly different tunneling matrix elements. To decide the issue, future DFT calculations should include the observed surface reconstructions.

https://dx.doi.org/10.1021/acs.jpclett.0c02711
J. Phys. Chem. Lett. 2020, 11, 9393−9399

Complete STS maps were performed in the region shown in Figure 2b; the results are presented in Figure 4. The color-coded plot in Figure 4b presents the spatial evolution of the tunneling DOS over the 15 nm line crossing the boundary between two regions of different reconstructions (see also Supplementary Figure 3). The gap at zero bias (colored blue) is a quite constant feature. However, the overall spectral background is different in the two regions and even varies on an atomic scale in the 1 × 2 region (yellow-red oscillations better seen at positive bias). Another intriguing result is the discovery of an electronic ordering (Figure 4c). It is observed at negative bias (occupied sample states) and only in $\sqrt{2} \times \sqrt{2}$ reconstructed regions (Figure 4) (see also Supplementary Figure 4). The autocorrelation presented in the inset clearly shows two satellite peaks in the Fe−Fe direction separated by ∼5 nm (approximately eight Fe−Fe interatomic distances). This modulation is reminiscent of that observed in Ca-122 and attributed to the nematic order.[39] However, many questions remain. Why was the electronic modulation not observed in 1 × 2 regions? Why does it appear only at negative bias? Why is it unidimensional? These questions along with the identification of impurities clearly observed in STS data (red and dark-blue spots) remain well beyond the scope of this study.

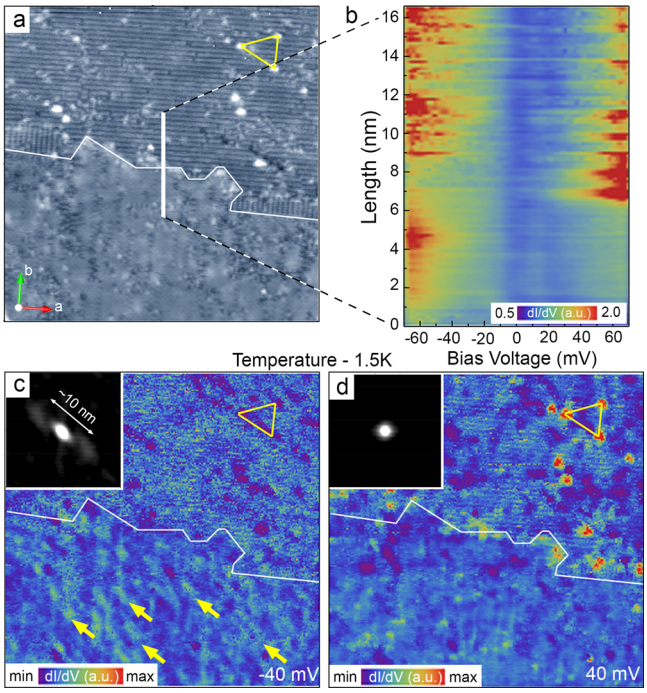

Figure 4. Spatial variations of electronic signatures. (a) A 50 nm × 50 nm STM image (V_T = −20 mV, and I_T = −900 pA), from the same location as in Figure 2b. The thin line depicts the boundary between the 1 × 2 (top) and $\sqrt{2} \times \sqrt{2}$ (bottom) regions. (b) Evolution of $dI/dV(V)$ spectra (color-coded) along the scan presented by the thick line in panel a. (c and d) $dI/dV(x, y, V)$ maps at V = −40 mV and V = 40 mV, respectively. In the insets, autocorrelation maps reveal a spatial electronic modulation of ∼5 nm of the occupied states of the sample. The yellow triangles define the positions of three atomic defects for identifying topography and spectroscopy maps.

With regard to the superconducting gap, its spectral smearing and strong filling are in striking contrast with fully open multiple gaps observed by *k*-selective ARPES.[28] In our case, the strong gap filling makes impossible the check of the multiband character of superconductivity; also, it obscures the information about possible nodes or other signatures of nontrivial pairing. Phenomenologically, gap filling can be taken into account by considering a pair-breaking Γ that accounts for a finite quasiparticle lifetime.[52] Γ enters the BCS formula for the superconducting DOS by substituting $E \rightarrow E - i\Gamma$: $\mathrm{DOS}(E) = \mathrm{Re}\{E - i\Gamma/\sqrt{(E - i\Gamma)^2 - \Delta^2}\}$ In Figure 1d, the dashed line represents the best fit achieved using the Dynes formula. The obtained superconducting gap energy Δ_{fit} of 6.8 meV is consistent with a superconducting critical temperature T_c of 35 K of $RbEuFe_4As_4$ ($2\Delta_{fit}/k_BT_c \simeq 4.5$). However, the fit of an almost completely filled gap required a very large parameter Γ_{fit} = 9.5 meV ≃ Δ_{fit}. This needs to be physically justified, as the microscopic phenomena behind it are the origin of the discrepancies between STS and ARPES results. Eventually, very different probe electron energies (a few millielectronvolts around the Fermi energy in the case of STS, several hundreds of electronvolts in the case of ARPES) might result in different interactions with the matter, in particular, with a very fragile reconstructed layer (that we demonstrated above). It could lead to inelastic terms in tunneling. In the future, a more detailed study of this question is necessary. Note that strong gap fillings have been previously revealed in other Fe-based superconducting pnictides;[54,55] the physical origin of this common phenomenon is currently being debated. In the case of $RbEuFe_4As_4$, the presence of magnetism makes the puzzle even more complex to solve.

In conclusion, owing to in situ cleavage at low temperatures, STM/STS experiments performed on single crystals of $RbEuFe_4As_4$ revealed the coexistence of large Rb- and Eu-terminated atomic terraces. Despite the different electronic properties of Rb and Eu atoms, the same reconstructions, 1 × 2 and $\sqrt{2} \times \sqrt{2}$, were observed on both types of surfaces, thus pointing to the essential role played by crystal symmetry in the reconstruction process. Below 35 K, a gap at zero bias related to superconducting order was observed. Although the estimated gap energy is above the BCS weak coupling value, the gap in the tunneling spectra is not fully open. Even at low temperatures ($T/T_c \simeq 0.05$), ∼90% of quasiparticle excitations remain. On $\sqrt{2} \times \sqrt{2}$ reconstructed terraces, STS revealed a long-range quasiperiodic ordering of the occupied states with energies 10−50 meV below the Fermi level. The data acquired in a wider energy window of ±2.5 eV were compared to DFT calculations; the observed spectral peak at −1.8 V was attributed to the deep-lying Eu 4f level; no other important contribution of Eu to the electronic bands was found. We thus conclude that Eu in $RbEuFe_4As_4$ does not contribute directly to Cooper pair formation.

■ ASSOCIATED CONTENT

Supporting Information

The Supporting Information is available free of charge at https://pubs.acs.org/doi/10.1021/acs.jpclett.0c02711.

Sample preparation and STM study, DFT calculations, additional references, and Supplementary Figures 1−4 (PDF)

https://dx.doi.org/10.1021/acs.jpclett.0c02711
J. Phys. Chem. Lett. 2020, 11, 9393−9399

AUTHOR INFORMATION

Corresponding Author

Vasily S. Stolyarov − *Moscow Institute of Physics and Technology, Dolgoprudny 141700, Moscow, Russia; Dukhov Research Institute of Automatics (VNIIA), 127055 Moscow, Russia;* orcid.org/0000-0002-5317-0818; Email: vasiliy.stoliarov@gmail.com

Authors

Kirill S. Pervakov − *Ginzburg Center for High Temperature Superconductivity and Quantum Materials, Lebedev Physical Institute, 119991 Moscow, Russia*

Anna S. Astrakhantseva − *Moscow Institute of Physics and Technology, Dolgoprudny 141700, Moscow, Russia*

Igor A. Golovchanskiy − *Moscow Institute of Physics and Technology, Dolgoprudny 141700, Moscow, Russia; National University of Science and Technology MISIS, 119049 Moscow, Russia;* orcid.org/0000-0001-9469-037X

Denis V. Vyalikh − *Donostia International Physics Center (DIPC), 20018 Donostia-San Sebastián, Basque Country, Spain; IKERBASQUE, Basque Foundation for Science, 48013 Bilbao, Spain;* orcid.org/0000-0001-9053-7511

Timur K. Kim − *Diamond Light Source, Didcot OX11 0DE, United Kingdom;* orcid.org/0000-0003-4201-4462

Sergey V. Eremeev − *Institute of Strength Physics and Materials Science, Russian Academy of Sciences, 634055 Tomsk, Russia;* orcid.org/0000-0002-9477-3017

Vladimir A. Vlasenko − *Ginzburg Center for High Temperature Superconductivity and Quantum Materials, Lebedev Physical Institute, 119991 Moscow, Russia*

Vladimir M. Pudalov − *Ginzburg Center for High Temperature Superconductivity and Quantum Materials, Lebedev Physical Institute, 119991 Moscow, Russia; National Research University Higher School of Economics, 101000 Moscow, Russia*

Alexander A. Golubov − *Moscow Institute of Physics and Technology, Dolgoprudny 141700, Moscow, Russia; Faculty of Science and Technology and MESA+, Institute of Nanotechnology, 7500 AE Enschede, The Netherlands*

Eugene V. Chulkov − *Donostia International Physics Center (DIPC), 20018 Donostia-San Sebastián, Basque Country, Spain; National Research University Higher School of Economics, 101000 Moscow, Russia*

Dimitri Roditchev − *Laboratoire de Physique et d'Etude des Materiaux, LPEM, UMR-8213, ESPCI-Paris, PSL, CNRS, Sorbonne University, 75005 Paris, France*

Complete contact information is available at: https://pubs.acs.org/10.1021/acs.jpclett.0c02711

Author Contributions

V.S.S. conceived the project and supervised the STM/STS experiments. V.S.S. and A.S.A. performed the STM/STS study. K.S.P. and V.A.V. grew the crystals. A.S.A. and A.A.G. independently measured magnetic properties. S.V.E. and E.V.C. performed DFT calculations. V.S.S., D.V.V., T.K.K., S.V.E., V.M.P., A.A.G., E.V.C., and D.R. provided the explanation of the observed effects. V.S.S. and D.R. wrote the paper with essential contributions from other authors.

Notes

The authors declare no competing financial interest.

ACKNOWLEDGMENTS

The authors are grateful to D. Baranov, S. Kozlov, and D. Kasatonov for technical support. The work was supported by Russian Science Foundation Grant 18-72-10118. D.R. acknowledges French ANR Grant SUPERSTRIPES. D.R. acknowledge COST Action CA16218 (Nanoscale Coherent Hybrid Devices for Superconducting Quantum Technologies). S.V.E. acknowledges the Government research assignment for ISPMS SB RAS, Project III.23.2.9. The authors also acknowledge support from the Spanish Ministry of Economy (MAT-2017-88374-P). K.S.P. and V.A.V. acknowledge support within the state assignment of the Ministry of Science and Higher Education of the Russian Federation (Project "Physics of high-temperature superconductors and novel quantum materials", 0023-2019-0005). V.M.P. acknowledges support by RFBR (Project 18-02-01013).

REFERENCES

(1) Bulaevskii, L. N.; Buzdin, A. I.; Kulić, M. L.; Panjukov, S. V. Coexistence of Superconductivity and Magnetism Theoretical Predictions and Experimental Results. *Adv. Phys.* **1985**, *34*, 175−261.

(2) Flouquet, J.; Buzdin, A. Ferromagnetic Superconductors. *Phys. World* **2002**, *15*, 41−46.

(3) Lyuksyutov, I. F.; Pokrovsky, V. L. Ferromagnet−Superconductor Hybrids. *Adv. Phys.* **2005**, *54*, 67−136.

(4) Buzdin, A. I. Proximity Effects in Superconductor-Ferromagnet Heterostructures. *Rev. Mod. Phys.* **2005**, *77*, 935−976.

(5) Bergeret, F. S.; Volkov, A. F.; Efetov, K. B. Odd Triplet Superconductivity and Related Phenomena in Superconductor-Ferromagnet Structures. *Rev. Mod. Phys.* **2005**, *77*, 1321−1373.

(6) Aoki, D.; Flouquet, J. Ferromagnetism and Superconductivity in Uranium Compounds. *J. Phys. Soc. Jpn.* **2012**, *81*, 011003.

(7) Paulsen, C.; Hykel, D. J.; Hasselbach, K.; Aoki, D. Observation of the Meissner-Ochsenfeld Effect and the Absence of the Meissner State in UCoGe. *Phys. Rev. Lett.* **2012**, *109*, 237001.

(8) Paglione, J.; Greene, R. High-Temperature Superconductivity in Iron-Based Materials. *Nat. Phys.* **2010**, *6*, 645−658.

(9) Si, Q.; Yu, R.; Abrahams, E. High-Temperature Superconductivity in Iron Pnictides and Chalcogenides. *Nat. Rev. Mater.* **2016**, *1*, 16017.

(10) Dutta, A.; Anupam; Hossain, Z.; Gupta, A. K. A Temperature Dependent Tunneling Study of the Spin Density Wave Gap in $EuFe_2As_2$ Single Crystals. *J. Phys.: Condens. Matter* **2013**, *25*, 375602.

(11) Ren, Z.; Tao, Q.; Jiang, S.; Feng, C.; Wang, C.; Dai, J.; Cao, G.; Xu, Z. Superconductivity Induced by Phosphorus Doping and its Coexistence with Ferromagnetism in $EuFe_2(As_{0.7}P_{0.3})_2$. *Phys. Rev. Lett.* **2009**, *102*, 137002.

(12) Cao, G.; Xu, S.; Ren, Z.; Jiang, S.; Feng, C.; Xu, Z. Superconductivity and Ferromagnetism in $EuFe_2(As_{1-x}P_x)_2$. *J. Phys.: Condens. Matter* **2011**, *23*, 464204.

(13) Nowik, I.; Felner, I.; Ren, Z.; Cao, G. H.; Xu, Z. A. Coexistence of Ferromagnetism and Superconductivity: Magnetization and Mössbauer Studies of $EuFe_2(As_{1-x}P_x)_2$. *J. Phys.: Condens. Matter* **2011**, *23*, 065701.

(14) Zapf, S.; Wu, D.; Bogani, L.; Jeevan, H. S.; Gegenwart, P.; Dressel, M. Varying Eu^{2+} Magnetic Order by Chemical Pressure in $EuFe_2(As_{1-x}P_x)_2$. *Phys. Rev. B* **2011**, *84*, 140503.

(15) Zapf, S.; Jeevan, H. S.; Ivek, T.; Pfister, F.; Klingert, F.; Jiang, S.; Wu, D.; Gegenwart, P.; Kremer, R. K.; Dressel, M. $EuFe_2(As_{1-x}P_x)_2$: Reentrant Spin Glass and Superconductivity. *Phys. Rev. Lett.* **2013**, *110*, 237002.

(16) Stolyarov, V. S. Domain Meissner State and Spontaneous Vortex-Antivortex Generation in the Ferromagnetic Superconductor $EuFe_2(As_{0.79}P_{0.21})_2$. *Sci. Adv.* **2018**, *4*, eaat1061.

(17) Nandi, S.; Jin, W. T.; Xiao, Y.; Su, Y.; Price, S.; Shukla, D. K.; Strempfer, J.; Jeevan, H. S.; Gegenwart, P.; Brückel, T. Coexistence of

Superconductivity and Ferromagnetism in P-doped $EuFe_2As_2$. *Phys. Rev. B* **2014**, *89*, 014512.
(18) Devizorova, Z.; Mironov, S.; Buzdin, A. Theory of Magnetic Domain Phases in Ferromagnetic Superconductors. *Phys. Rev. Lett.* **2019**, *122*, 117002.
(19) Ghigo, G.; Torsello, D.; Gozzelino, L.; Tamegai, T.; Veshchunov, I. S.; Pyon, S.; Jiao, W.; Cao, G.-H.; Grebenchuk, S. Y.; Golovchanskiy, I. A.; Stolyarov, V. S.; Roditchev, D. Microwave Analysis of the Interplay Between Magnetism and Superconductivity in $EuFe_2(As_{1-x}P_x)_2$ Single Crystals. *Phys. Rev. Research* **2019**, *1*, 033110.
(20) Grebenchuk, S. Y.; Devizorova, Z. A.; Golovchanskiy, I. A.; Shchetinin, I. V.; Cao, G.-H.; Buzdin, A. I.; Roditchev, D.; Stolyarov, V. S. Crossover from Ferromagnetic Superconductor to Superconducting Ferromagnet in P-doped $EuFe_2(As_{1-x}P_x)_2$. *Phys. Rev. B* **2020**, *102*, 144501.
(21) Kawashima, K.; Ishida, S.; Fujihisa, H.; Gotoh, Y.; Kihou, K.; Yoshida, Y.; Eisaki, H.; Ogino, H.; Iyo, A. Superconductivity in a New 1144-Type Family of (La,Na)AFe4As4 (A = Rb or Cs). *J. Phys. Chem. Lett.* **2018**, *9*, 868−873.
(22) Bao, J.-K.; Willa, K.; Smylie, M. P.; Chen, H.; Welp, U.; Chung, D. Y.; Kanatzidis, M. G. Single Crystal Growth and Study of the Ferromagnetic Superconductor $RbEuFe_4As_4$. *Cryst. Growth Des.* **2018**, *18*, 3517−3523.
(23) Liu, Y.; Liu, Y.-B.; Tang, Z.-T.; Jiang, H.; Wang, Z.-C.; Ablimit, A.; Jiao, W.-H.; Tao, Q.; Feng, C.-M.; Xu, Z.-A.; Cao, G.-H. Superconductivity and Ferromagnetism in Hole-Doped $RbEuFe_4As_4$. *Phys. Rev. B* **2016**, *93*, 214503.
(24) Jiang, H.; Sun, Y.-L.; Xu, Z.-A.; Cao, G.-H. Crystal Chemistry and Structural Design of Iron-Based Superconductors. *Chin. Phys. B* **2013**, *22*, 087410.
(25) Iyo, A.; Kawashima, K.; Kinjo, T.; Nishio, T.; Ishida, S.; Fujihisa, H.; Gotoh, Y.; Kihou, K.; Eisaki, H.; Yoshida, Y. New-structure-type Fe-based superconductors: $CaAFe_4As_4$ (A = K, Rb, Cs) and $Sr_AFe_4As_4$ (A = Rb, Cs). *J. Am. Chem. Soc.* **2016**, *138*, 3410−3415.
(26) Kawashima, K.; Kinjo, T.; Nishio, T.; Ishida, S.; Fujihisa, H.; Gotoh, Y.; Kihou, K.; Eisaki, H.; Yoshida, Y.; Iyo, A. Superconductivity in Fe-Based Compound $EuAFe_4As_4$ (A = Rb and Cs). *J. Phys. Soc. Jpn.* **2016**, *85*, 064710.
(27) Liu, Y.; Liu, Y.-B.; Chen, Q.; Tang, Z.-T.; Jiao, W.-H.; Tao, Q.; Xu, Z.-A.; Cao, G.-H. A New Ferromagnetic Superconductor: $CsEuFe_4As_4$. *Sci. Bull.* **2016**, *61*, 1213−1220.
(28) Kim, T. K.; Pervakov, K.; Evtushinsky, D.; Jung, S.; Poelchen, G.; Kummer, K.; Vlasenko, V. A.; Roditchev, D.; Stolyarov, V.; Vyalikh, D.; Borisov, V.; Valenti, R.; Ernst, A.; Eremeev, S.; Chulkov, E. When Superconductivity Does Not Fear Magnetism: Insight Into Electronic and Magnetic Structure of $RbEuFe_4As_4$. *arXiv* **2020**, 2008.00736.
(29) Hemmida, M. Topological Magnetic Order and Superconductivity in $RbEuFe_4As_4$. *arXiv* **2020**, 2010.02110.
(30) Stolyarov, V. S.; et al. Unique Interplay Between Superconducting and Ferromagnetic Orders in $EuRbFe_4As_4$. *Phys. Rev. B* **2018**, *98*, 140506.
(31) Willa, K.; Willa, R.; Bao, J.-K.; Koshelev, A. E.; Chung, D. Y.; Kanatzidis, M. G.; Kwok, W.-K.; Welp, U. Strongly Fluctuating Moments in The High-Temperature Magnetic Superconductor $RbEuFe_4As_4$. *Phys. Rev. B* **2019**, *99*, 180502.
(32) Iida, K.; et al. Coexisting Spin Tesonance and Long-Range Magnetic Order of Eu in $EuRbFe_4As_4$. *Phys. Rev. B* **2019**, *100*, 014506.
(33) Xiang, L.; Bud'ko, S. L.; Bao, J.-K.; Chung, D. Y.; Kanatzidis, M. G.; Canfield, P. C. Pressure-Temperature Phase Diagram of the $EuRbFe_4As_4$ Superconductor. *Phys. Rev. B* **2019**, *99*, 144509.
(34) Koshelev, A. E.; Willa, K.; Willa, R.; Smylie, M. P.; Bao, J.-K.; Chung, D. Y.; Kanatzidis, M. G.; Kwok, W.-K.; Welp, U. Melting of Vortex Lattice in The Magnetic Superconductor $RbEuFe_4As_4$. *Phys. Rev. B* **2019**, *100*, 094518.
(35) Devizorova, Z.; Buzdin, A. Superconductivity-Driven Helical Magnetic Structure in $EuRbFe_4As_4$ Ferromagnetic Superconductor. *Phys. Rev. B* **2019**, *100*, 104523.
(36) Koshelev, A. E. Helical Structures in Layered Magnetic Superconductors Due to Indirect Exchange Interactions Mediated by Interlayer Tunneling. *Phys. Rev. B* **2019**, *100*, 224503.
(37) Johnston, D. C. The Puzzle of High Temperature Superconductivity in Layered Iron Pnictides and Chalcogenides. *Adv. Phys.* **2010**, *59*, 803−1061.
(38) Pogrebna, A.; Mertelj, T.; Vujičić, N.; Cao, G.; Xu, Z. A.; Mihailovic, D. Coexistence of Ferromagnetism and Superconductivity in Iron Based Pnictides: A Time Resolved Magnetooptical Study. *Sci. Rep.* **2015**, *5*, 7754.
(39) Chuang, T.-M.; Allan, M. P.; Lee, J.; Xie, Y.; Ni, N.; Bud'ko, S. L.; Boebinger, G. S.; Canfield, P. C.; Davis, J. C. Nematic Electronic Structure in The "Parent" State of The Iron-Based Superconductor $Ca(Fe_{1-x}Co_x)_2As_2$. *Science* **2010**, *327*, 181−184.
(40) Gao, M.; Ma, F.; Lu, Z.-Y.; Xiang, T. Surface Structures of Ternary Iron Arsenides AFe_2As_2 (*A* = Ba, Sr, or Ca). *Phys. Rev. B* **2010**, *81*, 193409.
(41) Li, L.; Zheng, Q.; Zou, Q.; Rajput, S.; Ijaduola, A. O.; Wu, Z.; Wang, X. P.; Cao, H. B.; Somnath, S.; Jesse, S.; Chi, M.; Gai, Z.; Parker, D.; Sefat, A. S. Improving Superconductivity in $BaFe_2As_2$-based Crystals by Cobalt Clustering and Electronic Uniformity. *Sci. Rep.* **2017**, *7*, 949.
(42) Massee, F.; Huang, Y.; Huisman, R.; de Jong, S.; Goedkoop, J. B.; Golden, M. S. Nanoscale superconducting-gap variations and lack of phase separation in optimally doped $BaFe_{1.86}Co_{0.14}As_2$. *Phys. Rev. B* **2009**, *79*, 220517.
(43) Massee, F.; de Jong, S.; Huang, Y.; Kaas, J.; van Heumen, E.; Goedkoop, J. B.; Golden, M. S. Cleavage Surfaces of the $BaFe_{2-x}Co_xAs_2$ and $Fe_ySe_{1-x}Te_x$ Superconductors: A Combined STM Plus LEED Study. *Phys. Rev. B* **2009**, *80*, 140507.
(44) Yin, Y.; Zech, M.; Williams, T. L.; Wang, X. F.; Wu, G.; Chen, X. H.; Hoffman, J. E. Scanning Tunneling Spectroscopy and Vortex Imaging In The Iron Pnictide Superconductor $BaFe_{1.8}Co_{0.2}As_2$. *Phys. Rev. Lett.* **2009**, *102*, 097002.
(45) Yin, Y.; Zech, M.; Williams, T.; Hoffman, J. Scanning Tunneling Microscopy and Spectroscopy on Iron-Pnictides. *Phys. C* **2009**, *469*, 535−544.
(46) Nascimento, V. B.; et al. Surface Geometric and Electronic Structures of $BaFe_2As_2(001)$. *Phys. Rev. Lett.* **2009**, *103*, 076104.
(47) Zhang, H.; Dai, J.; Zhang, Y.; Qu, D.; Ji, H.; Wu, G.; Wang, X. F.; Chen, X. H.; Wang, B.; Zeng, C.; Yang, J.; Hou, J. G. $\sqrt{2} \times \sqrt{2}$ Structure and Charge Inhomogeneity at The Surface of Superconducting.$BaFe_{2-x}Co_xAs_2$(x = 0−0.32). *Phys. Rev. B* **2010**, *81*, 104520.
(48) Nishizaki, T.; Nakajima, Y.; Tamegai, T.; Kobayashi, N. Surface Structure and Superconductivity in $Ba(Fe_{0.93}Co_{0.07})_2As_2$ Probed by Scanning Tunneling microscopy/spectroscopy. *J. Phys. Soc. Jpn.* **2011**, *80*, 014710.
(49) Zou, Q.; Fu, M.; Wu, Z.; Li, L.; Parker, D. S.; Sefat, A. S.; Gai, Z. Competitive and Cooperative Electronic States in $Ba(Fe_{1-x}T_x)_2As_2$ with T = Co, Ni, Cr. *arXiv* **2020**, 1908.10436.
(50) Boyer, M. C.; Chatterjee, K.; Wise, W. D.; Chen, G. F.; Luo, J. L.; Wang, N. L.; Hudson, E. W. Scanning tunneling microscopy of the 32 K superconductor $(Sr_{1-x}K_x)Fe_2As_2$. *arXiv* **2020**, 0806.4400.
(51) Niestemski, F. C.; Nascimento, V. B.; Hu, B.; Plummer, W.; Gillett, J.; Sebastian, S.; Wang, Z.; Madhavan, V. Unveiling the Atomic and Electronic Structure at the Surface of the Parent Pnictide $SrFe_2As_2$. *arXiv* **2020**, 0906.2761.
(52) Dynes, R. C.; Narayanamurti, V.; Garno, J. P. Direct Measurement of Quasiparticle-Lifetime Broadening in a Strong-Coupled Superconductor. *Phys. Rev. Lett.* **1978**, *41*, 1509−1512.
(53) Vlasenko, V.; Pervakov, K.; Gavrilkin, S. Vortex Pinning and Magnetic Phase Diagram of $EuRbFe_4As_4$ Iron-Based Superconductor. *Supercond. Sci. Technol.* **2020**, *33*, 084009.
(54) Massee, F.; Huang, Y. K.; Kaas, J.; van Heumen, E.; de Jong, S.; Huisman, R.; Luigjes, H.; Goedkoop, J. B.; Golden, M. S. Pseudo

https://dx.doi.org/10.1021/acs.jpclett.0c02711
J. Phys. Chem. Lett. 2020, 11, 9393−9399

Gap-Less High-T_C Superconductivity in $BaCo_xFe_{2-x}As_2$. *EPL (Europhysics Letters)* **2010**, *92*, 57012.
(55) Li, A.; et al. Surface Terminations and Layer-Resolved Tunneling Spectroscopy of the 122 Iron Pnictide Superconductors. *Phys. Rev. B* **2019**, *99*, 134520.

https://dx.doi.org/10.1021/acs.jpclett.0c02711
J. Phys. Chem. Lett. 2020, 11, 9393−9399